

Fully integrated InGaAs/InP single-photon detector module with gigahertz sine wave gating

Xiao-Lei Liang,¹ Jian-Hong Liu,² Quan Wang,² De-Bing Du,² Jian Ma,¹ Ge Jin,¹
Zeng-Bing Chen,¹ Jun Zhang,^{1, a)} and Jian-Wei Pan¹

¹⁾*Hefei National Laboratory for Physical Sciences at Microscale and Department of Modern Physics, University of Science and Technology of China, Hefei, Anhui 230026, China*

²⁾*Anhui Quantum Communication Technology Co., Ltd., Hefei, Anhui 230088, China*

(Dated: 21 February 2022)

InGaAs/InP single-photon avalanche diodes (SPADs) working in the regime of GHz clock rates are crucial components for the high-speed quantum key distribution (QKD). We have developed for the first time a compact, stable and user-friendly tabletop InGaAs/InP single-photon detector system operating at a 1.25 GHz gate rate that fully integrates functions for controlling and optimizing SPAD performance. We characterize the key parameters of the detector system and test the long-term stability of the system for continuous operation of 75 hours. The detector system can substantially enhance QKD performance and our present work paves the way for practical high-speed QKD applications.

^{a)}Electronic mail: zhangjun@ustc.edu.cn

I. INTRODUCTION

For applications requiring near-infrared single-photon detection such as quantum key distribution (QKD)¹, optical time domain reflectometry² and eye-safe laser ranging³, InGaAs/InP single-photon avalanche diodes (SPADs) working in the Geiger mode are widely used due to their practicality⁴. Numerous works on quenching techniques and afterpulsing reduction for single-photon detection have been performed over the past two decades. Afterpulsing refers to undesired subsequent avalanches that are due to the depopulation of the trapped charge carriers created during previous avalanches. Suppressing the afterpulsing effect is a key step to improve SPAD performance. The afterpulse probability can be roughly modeled as⁵

$$P_{ap} \propto (C_d + C_{par}) \int_0^{\Delta t} V_{ex}(t) dt \times e^{-T_d/\tau}, \quad (1)$$

where C_d is the diode capacitance, C_{par} is the parasitic capacitance, Δt is the avalanche duration time, V_{ex} is the excess bias, T_d is the deadtime, and τ is the lifetime of detrapping carriers. According to Eq. 1, there are several approaches to reduce afterpulsing. Increasing the operating temperature (T) in order to decrease τ , or increasing T_d , can both reduce the release rate of the trapped carriers. However, higher temperatures deteriorate the dark count performance while longer deadtime settings limit the maximum count rate. Minimizing C_{par} can reduce afterpulsing by decreasing the avalanche charge quantity. This has been demonstrated, for instance, in experiments using integrated quenching electronics⁵ or the hybrid packaging technique⁶. Nevertheless, these sophisticated techniques are challenging. Significantly reducing Δt can also effectively limit the avalanche charge quantity, which is the original idea of the recently emerging technique called rapid gating^{7–15}.

Once the afterpulsing effect is significantly suppressed, InGaAs/InP SPADs can operate in the high-speed mode. For applications like QKD, high repetition frequency is critical for key generation. Such high-speed QKD experiments using rapid gating detectors have recently been demonstrated^{16–19}. In rapid gating schemes, due to an ultrashort gating duration, avalanche charge quantity is extremely limited. As a result, the afterpulsing effect is sufficiently reduced, and the gating frequency can easily reach the GHz level. Low charge flow however, creates a weak avalanche signal to be detected. There are currently two approaches to extract weak avalanches from huge capacitive response signals: sine wave gating and filtering^{7–12}, and self-differencing^{13,14}.

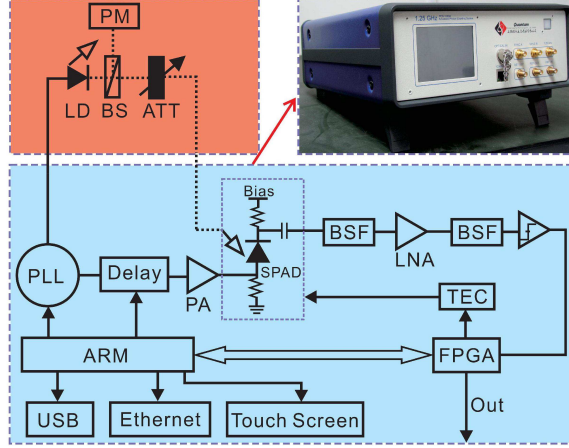


FIG. 1. Experimental setup for single-photon characterization (top left), detector system photo (top right), and detector system diagram (bottom). See text for explanation.

II. DETECTOR SYSTEM DESIGN

In order to be effectively and reliably applied in practical QKD applications, a compact and stable rapid gating detector is indispensable. We have developed for the first time a fully integrated tabletop InGaAs/InP single-photon detector working at a gating frequency of 1.25 GHz (see Fig. 1). The practical features of the detector system include: multiple independently programmable high precision clock outputs, internal and external clock references, gate amplitude control, low-noise fine tuning bias, automatic delay adjustment for synchronized photon detection, switchable avalanche signal monitor, adjustable SPAD temperature, tunable discrimination threshold, programmable deadtime, and user-friendly interface. All system components are assembled into a module 25 cm \times 10 cm \times 33 cm in size as shown in Fig. 1.

The rapid gating scheme of the detector system is based on sine wave gating and filtering⁷⁻¹². A phase-locked loop (PLL) generates initial sine waves at a frequency of $f_g=1.25$ GHz. Using a power amplifier (PA) with a gain of 40 dB, the sine waves have a peak-peak amplitude (V_{pp}) of 10 V. V_{pp} may be further adjusted by a digital attenuator. The SPAD response signal initially passes through microwave band-stop filters (BSFs) at a center frequency of 1.25 GHz. The attenuated signal is then amplified by a low-noise amplifier (LNA) and subsequently filtered by the second set of BSFs. The capacitive response signal is then suppressed to a negligible level where the avalanche signal can be discriminated. An

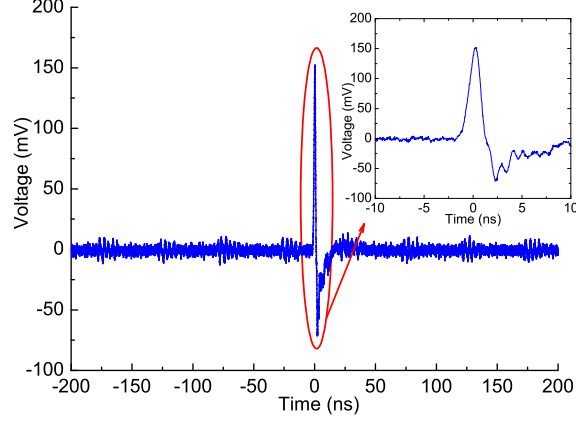


FIG. 2. Oscilloscope trace of the avalanche signal. Inset: expanded view of the main peak.

electronic switch also allows the avalanche signal to be monitored on an oscilloscope.

Fig. 2 shows a typical avalanche trace captured on a 12 GHz oscilloscope (Agilent infinii-ium). The avalanche amplitude is greater than 100 mV with the peak-peak electronic noise below 20 mV. This high signal-to-noise ratio is attributed to careful consideration of signal integrity in our circuit board design, good electrical shielding, and ultra-low noise bias with a root mean square ripple less than 800 μ V. The undershoot of the avalanche trace is due to the capacitive effect, since the output from SPAD is alternating current coupled with a capacitor.

In order to achieve the objectives of easy-to-use and stable long-term operation, auxiliary hardware and software designs are used to control the detector system. The control center is an advanced RISC machine (ARM) embedded system. The user interface is an on-board touch screen that communicates with an embedded system program developed in Nokia’s Qt framework. Alternatively, a computer can control the detector system either via universal serial bus (USB), or remotely via ethernet. A field-programmable gate array (FPGA) and a thermoelectric cooling (TEC) driver are used to maintain SPAD temperature. FPGA can also perform counting, and apply logic deadtime to the output of the discriminator. Logic deadtime refers to the “count-off time” as discussed in Ref.^{9,10}. Unlike real deadtime, during which the SPAD is not operating in the Geiger mode, logic deadtime only prevents counting for a period after a primary detection^{9,10}.

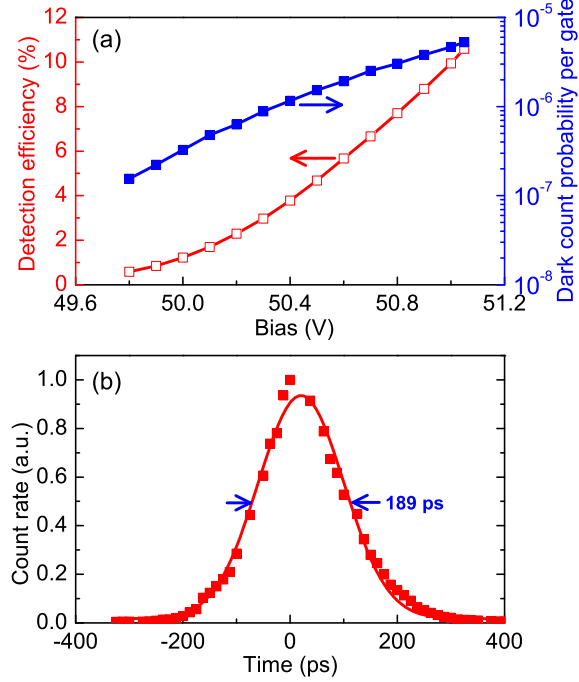


FIG. 3. (a) Detection efficiency (η) and dark count probability per gate (P_{dc}) as a function of bias. (b) Effective gating width measurement by scanning the relative delay between optical pulses and sine gates at $\eta=10\%$.

III. CHARACTERIZATION AND DISCUSSION

For SPAD characterization, an optical test bench is constructed as shown in Fig. 1. A laser diode (LD, picoquant PDL 800-D) is triggered by the PLL synchronized output at a frequency of $f_l = f_g/100$. The ultrashort optical pulses are divided by an asymmetric beam splitter (BS). The optical power in one of the BS output ports is monitored by a calibration power meter (PM, IQS-1500). A LabVIEW program reads the measurement results of the PM and regulates a precise variable attenuator (ATT, IQS-3150) in real time in order to cancel the intensity fluctuations of the LD. The intensity of the resulting optical pulses reach the single-photon level.

Fig. 3(a) shows the efficiency-noise performance of the SPAD under the operating conditions of $T=-50^\circ\text{C}$ and a mean photon number per optical pulse of $\mu=1$. As the bias rises the system detection efficiency (η) increases linearly while the dark count probability per gate (P_{dc}) increases exponentially. When $\eta=10\%$, P_{dc} is 4.66×10^{-6} , corresponding to 5.83 kHz dark count rate. The effective gating width at $\eta=10\%$ is measured by scanning the

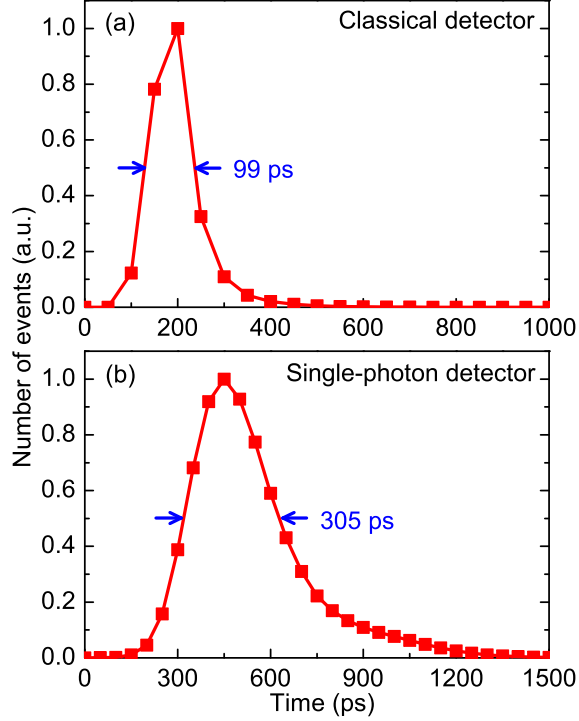


FIG. 4. (a) The overall jitter of LD, PLL, and the TDC electronics measured with a 12.5 GHz InGaAs PIN detector. The jitter of the classical detector is negligible. (b) The overall jitter measured with the rapid gating InGaAs single-photon detector at $\eta=10\%$.

relative delay between optical pulses and sine gates. The results are plotted and fitted in Fig. 3(b). The full width at half maximum of the gating width is 189 ps, and the resulting normalized dark count probability per ns at $\eta=10\%$ is 2.47×10^{-5} . This is consistent with the results that are obtained with the same InGaAs/InP SPAD using a conventional low-frequency gating technique (10 kHz gating frequency and 10 ns gating width) under the same conditions of T and η . This similarity suggests that dark count performance of SPAD is independent of the quenching techniques.

Timing resolution is a key parameter of SPAD for high-speed applications. The intrinsic jitter of the system is measured with a 12.5 GHz InGaAs PIN photodetector (ET-3500F) using a multistop time to digital converter (TDC, Agilent Acqiris) of 50 ps timing resolution. The overall jitter including the contributions of LD, PLL, and TDC is 99 ps as shown in Fig. 4(a). The jitter of the whole detector system with the rapid gating SPAD at $\eta=10\%$ is measured to be 305 ps (see Fig. 4(b)). Therefore, the timing resolution of the rapid gating SPAD itself is $\sqrt{305^2 - 99^2} = 288$ ps. There are two reasons for this moderate timing

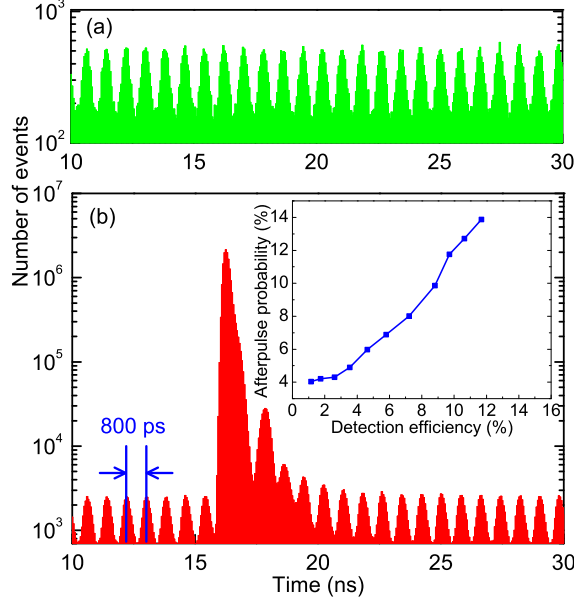


FIG. 5. The histogram of detection events under the conditions of $\eta=10\%$, $\mu=0.1$, $T=-50\text{ }^\circ\text{C}$ and a 10-minute integration time without (a) and with (b) optical illumination. Inset: P_{ap} versus η using the same bias settings as in Fig. 3(a).

resolution. First, this resolution includes contributions from the discrimination circuit and the FPGA, which are difficult to quantify separately. Second, in the rapid gating scheme, although the cascaded BSFs minimize capacitive response signals, they can also distort the avalanche signals. Such distortions add timing jitter²⁰.

For afterpulsing characterization, although the standard double-gate method⁵ is the most precise approach, it cannot be applied to rapid gating. In our experiment we use the high-speed TDC system to directly tag the timing of all the avalanche detections and then statistically analyze the events offline. At each bias setting we acquire the distribution of detection events both with and without optical illumination. The common measurement conditions include $f_l=12.5\text{ MHz}$, $\mu=0.1$, $T=-50\text{ }^\circ\text{C}$, a 10-minute integration time, and without applying logic deadtime^{9,10}. Histograms for $\eta=10\%$ are shown in Fig. 5. Fig. 5(a) shows an equal distribution of dark counts in which peaks are separated by 800 ps. Fig. 5(b) shows the corresponding histogram with the illumination of the pulsed laser. In this case, the main peak is due to photon detections and the subsequent decay shows the typical afterpulsing effect. For practical applications appropriate coincidence technique may be necessary to clearly separate the main peak and the first side peak.

In the experiment, the total afterpulse probability P_{ap} is calculated using

$$P_{ap} = \frac{C_{tol} - C_{dc} - C_{ph}}{C_{ph}}, \quad (2)$$

where C_{dc} is the number of dark counts in the case of non-illumination, and C_{tol} and C_{ph} are the numbers of total counts and photon counts, respectively, in the case of illumination. C_{ph} is estimated according to the counts in the main peaks after subtracting the contribution of dark counts, i.e., $C_{dc}/(f_g/f_l)=C_{dc}/100$. P_{ap} as a function of η is presented in the inset of Fig. 5(b). For $\eta=10\%$, P_{ap} is $\sim 11.7\%$. This moderate afterpulsing probability is expected if one considers the following facts. Empirically, the SPAD temperature of -50°C we used here is somewhat low for rapid gating. In addition, P_{ap} highly depends on count rate or average time interval of avalanche detections⁹. Therefore, considering the parameters of η and μ in the experiment, 11.7% is the integration of P_{ap} over $\sim 8\ \mu\text{s}$. If we roughly normalize this value to the number of gates during that average time interval⁹, the afterpulse probability per gate is $11.7\%/(8\ \mu\text{s}/800\ \text{ps}) \sim 1.2 \times 10^{-5}$, corresponding to 6.4×10^{-5} per ns, which is about $3P_{dc}$ and consistent with the measurements shown in Fig. 5. In practice, P_{ap} could be made negligible by means of applying long logic deadtime¹⁰.

Finally, we test the stability performance of the detector system related to practical applications. If there is no feedback functionality in the detector system, η decreases over time due to slight drifts of the relative phase between optical pulses and sine gates. In Fig. 6(a), η is initially 11% . It takes 75 minutes for η to degrade to 10% and 100 minutes to degrade to 9% . We designed an automatic peak search mechanism as feedback control to the detector system. Every 10 minutes of continuous operation the delay is scanned in the full range and set to the point of maximum count. This process takes about 1 minute. The detection duty cycle can be improved by prolonging the feedback time interval and optimizing the feedback algorithm. Using this feedback control the detector system is continuously operated over 75 hours as shown in Fig. 6(b). The stability tests show that the detector system is well suited for practical use, such as in the next generation high-speed QKD applications. The slight detection efficiency changes in Fig. 6(b) are not due to the time-division feedback control, but probably to the amplitude fluctuations of sine gates. In the future, we will apply the technique of automatic gain control for the PA to stabilize the gate amplitude.

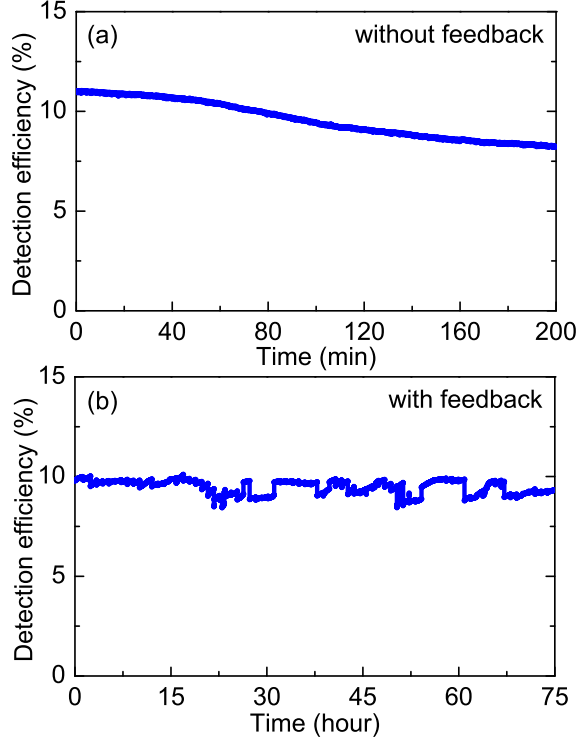


FIG. 6. The system stability test (a) without feedback control for short-term operation and (b) with feedback control for long-term operation.

IV. CONCLUSION

In summary, we have developed a 1.25 GHz gating tabletop InGaAs/InP single-photon detector system that integrates diverse functions required for practical applications. We have also characterized the SPAD performance and the long-term stability. Applying such detectors to QKD applications will significantly enhance QKD performance¹⁰.

ACKNOWLEDGMENTS

We acknowledge financial support from the CAS, the National High-Tech R&D Program, the National NSF of China, and the National Basic Research Program.

REFERENCES

¹N. Gisin, G. Ribordy, W. Tittel, and H. Zbinden, Rev. Mod. Phys. **74**, 145 (2002).

- ²P. Eraerds, M. Legre, J. Zhang, H. Zbinden, and N. Gisin, *J. Lightwave Technol.* **28**, 952 (2010).
- ³M. Ren, X. Gu, Y. Liang, W. Kong, E. Wu, G. Wu, and H. Zeng, *Opt. Express* **19**, 13497 (2011).
- ⁴M. A. Itzler, R. Ben-Michael, C.-F. Hsu, K. Slomkowski, A. Tosi, S. Cova, F. Zappa, and R. Ispasoiu, *J. Mod. Opt.* **54**, 283 (2007).
- ⁵J. Zhang, R. Thew, J.-D. Gautier, N. Gisin, and H. Zbinden, *IEEE J. Quantum Electron.* **45**, 792 (2009).
- ⁶M. Liu, C. Hu, J. C. Campbell, Z. Pan, and M. M. Tashima, *IEEE J. Quantum Electron.* **44**, 430 (2008).
- ⁷N. Namekata, S. Sasamori, and S. Inoue, *Opt. Express* **14**, 10043 (2006).
- ⁸N. Namekata, S. Adachi, and S. Inoue, *Opt. Express* **17**, 6275 (2009).
- ⁹J. Zhang, R. Thew, C. Barreiro, and H. Zbinden, *Appl. Phys. Lett.* **95**, 091103 (2009).
- ¹⁰J. Zhang, P. Eraerds, N. Walenta, C. Barreiro, R. Thew, and H. Zbinden, *Proc. SPIE* **7681**, 76810Z (2010).
- ¹¹P. Eraerds, E. Pomarico, J. Zhang, B. Sanguinetti, R. Thew, and H. Zbinden, *Rev. Sci. Instrum.* **81**, 103105 (2010).
- ¹²Y. Nambu, S. Takahashi, K. Yoshino, A. Tanaka, M. Fujiwara, M. Sasaki, A. Tajima, S. Yorozu, and A. Tomita, *Opt. Express* **19**, 20531 (2011).
- ¹³Z. L. Yuan, B. E. Kardynal, A. W. Sharpe, and A. J. Shields, *Appl. Phys. Lett.* **91**, 041114 (2007).
- ¹⁴Z. L. Yuan, A. W. Sharpe, J. F. Dynes, A. R. Dixon, and A. J. Shields, *Appl. Phys. Lett.* **96**, 071101 (2010).
- ¹⁵A. Tosi, A. D. Frera, A. B. Shehata, and C. Scarcella, *Rev. Sci. Instrum.* **83**, 013104 (2012).
- ¹⁶Z. L. Yuan, A. R. Dixon, J. F. Dynes, A. W. Sharpe, and A. J. Shields, *Appl. Phys. Lett.* **92**, 201104 (2008).
- ¹⁷A. R. Dixon, Z. L. Yuan, J. F. Dynes, A. W. Sharpe, and A. J. Shields, *Appl. Phys. Lett.* **96**, 161102 (2010).
- ¹⁸N. Namekata, G. Fujii, S. Inoue, T. Honjo, and H. Takesue, *Appl. Phys. Lett.* **91**, 011112 (2007).

¹⁹N. Namekata, H. Takesue, T. Honjo, Y. Tokura, and S. Inoue, Opt. Express **19**, 10632 (2011).

²⁰Y. Liang, E. Wu, X. Chen, M. Ren, Y. Jian, G. Wu, and H. Zeng, IEEE Photon. Technol. Lett. **23**, 887 (2011).